Proceedings of ASME Turbo Expo 2011
GT2011
June 6-10, 2011, Vancouver, British Columbia, Canada

GT2011-46364

WALL SHEAR STRESS MEASUREMENTS ON A HIGHLY LOADED COMPRESSOR CASCADE

Vincent Zander[*],
Christoph Dobriloff,
Mathias Lumpe,
Wolfgang Nitsche
Technische Universität Berlin
Strasse des 17. Juni 135
10623 Berlin, Germany
Email: vincent.zander@ilr.tu-berlin.de

ABSTRACT

This paper presents wall shear stress measurements obtained with a new type of wall-mounted probe based on the thermal electrical principle. The sensor consists of three single surface hot wires arranged in a delta configuration. This allows for measuring wall shear stress magnitude and direction simultaneously. Each probe has to be calibrated in a flat plate experiment for a number of wall shear values and flow directions before applying it to the relevant flow situation.

To assess the full potential of the newly designed sensors, they were applied to a low speed, large scale cascade test section equipped with highly loaded compressor blades. The high blade loading in conjunction with a small blade aspect ratio results in a strongly three-dimensional flow field with large secondary flow structures and flow separation. Furthermore, laminar separation bubbles can be observed on the blade surface. The wall shear stress distribution allows for resolving these existing flow structures and provides detailed insight into the flow on the blade's surface. The additionally measured flow direction reveals further details of the flow field.

Parallel to the experiments, RANS simulations were conducted using the commercial flow solver CFX to compare the simulated results with the measured values.

NOMENCLATURE

Geometric and Flow Quantities

$c_f = \tau_w/q_1$	$-$	skin friction coefficient
$c_p = p_x - p_1/q_1$	$-$	pressure coefficient
E	V	anemometer voltage
h	m	blade height
L	m	chord length
Ma	$-$	Mach number
p_t	Pa	total pressure
p	Pa	static pressure
q	Pa	dynamic pressure
Re	$-$	Reynolds number
s	m	length from leading edge
S_{max}	m	total length of blade suction side
t	m	pitch
u	m/s	velocity
x	m	coordinate in flow direction
y	m	coordinate in blade spanwise direction
β	deg	cascade inflow angle
γ	deg	stagger angle
δ	deg	flow angle
τ_w	Pa	wall shear stress

[*]Address all correspondence to this author.

Subscripts

B	bridge
1	inlet
2	outlet

INTRODUCTION

The wall shear stress is one of the major quantities in boundary layer theory. Its spatial and temporal development reveals a detailed picture of the boundary layer state. The magnitude and direction allow for an evaluation of the wall friction losses. Measuring the wall shear stress provides detailed information on the global and near wall flow topology. Due to this a lot of effort has been spent on developing measurement techniques to determine the wall shear stress. An overview of the existing techniques can be found in [2] and [3]. Most of these techniques are not suitable for turbomachinery applications. In [4] is given a summary of the measurement techniques that are used in turbomachine aerodynamics. Hot films are commonly used in turbomachines for measuring the wall shear stress. A major challenge using sensors based on thermoelectrical concepts is their calibration, especially on curved surfaces. As shown in [5] a calibration of hot films is not stringently required for observing transition and separation phenomena on turbomachinery blades. Even a so called quasi wall shear stress can be calculated from the anemometer output signals without calibration. However, a calibration is required when detailed boundary layer studies are conducted or for comparing measurement results with numerical simulations. Beside the magnitude of the wall shear stress vector, the measurement of the direction reveals further information on the flow topology. This provides for example detail information on secondary flow structures occurring on turbomachine blades. Approaches measuring magnitude and direction using a two-component hot film or hot wire sensor is presented in [6] and [7]. The sensor applied in the second paper allows an exact determination of the flow direction if the topology of the observed flow field is a priori known, because the calibration curves show multiple solutions for the flow direction. This drawback can be overcome using the newly developed wall shear stress sensor presented in [8]. It consists of three surface hot wires arranged in a delta configuration to measure the magnitude and direction of the wall shear stress vector. The use of surface hot wires instead of surface hot films has some particular advantages. The increased overheat ratios that can be used for hot wires reduce the influence of the fluid temperature on the measurements. Also the heat losses due to heat conduction to the substrate can be reduced by mounting the surface hot wire over a small cavity. Both factors result in an improved signal-to-noise ratio for the hot wire [9]. Asymmetrical design of the cavities allows for a distinct determination of the flow direction with the newly developed delta sensors.

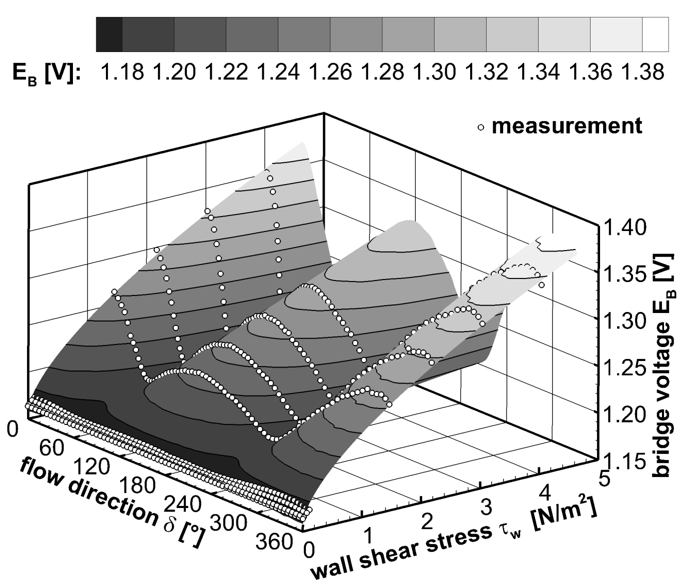

FIGURE 1: CALIBRATION SURFACE [1]

Experimental Setup

As already mentioned in the introduction, the delta sensors allow a distinct determination of the near wall flow direction using asymmetric cavities beneath the surface hot wires. A detailed description of the employed delta sensor layout can be found in [8] and [1]. A sketch of the probe design is also given in Fig. 5. The three surface hot wires are symmetrically placed

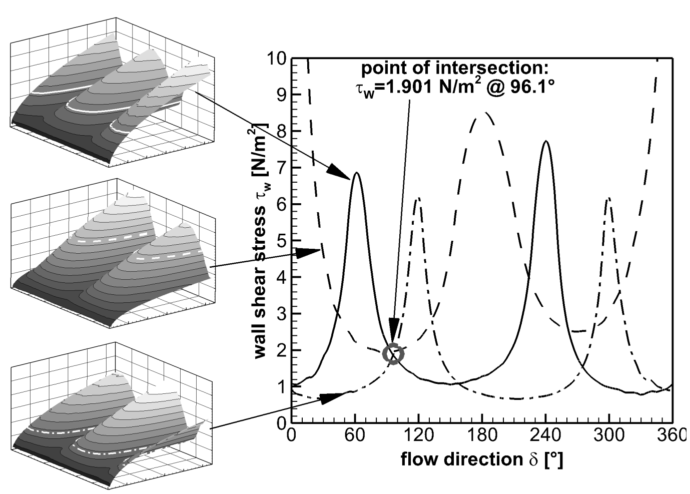

FIGURE 2: WALL SHEAR STRESS VECTOR IDENTIFICATION [1]

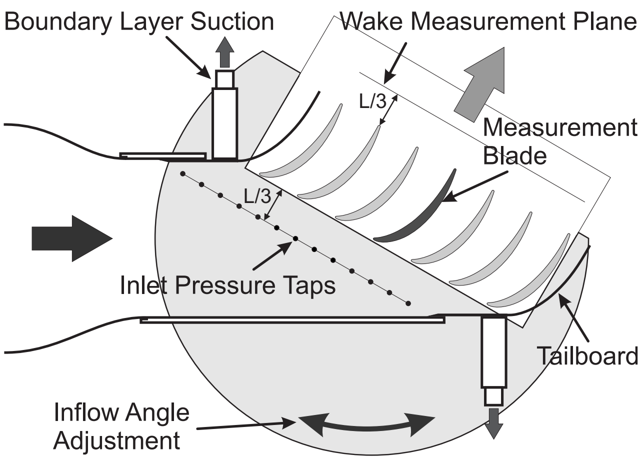

FIGURE 3: CASCADE TEST SECTION

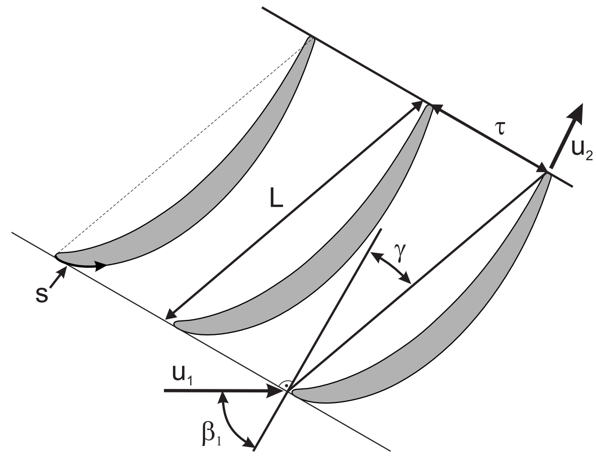

FIGURE 4: PROFILE GEOMETRY

on a circle with a diameter of $3.5mm$. The length of each hot wire is $1.5mm$. They cover a hexagonal area of $A = 9.1mm^2$. Concerning the blade sizes of the cascade test section described below and summarized in Table 1, the geometrical dimensions of the delta sensors are two orders of magnitude smaller. Therefore they are well-suited for the selected flow case. It can be seen that the delta sensors are flush-mounted to an insert with a diameter of $d = 10mm$. These inserts can be easily positioned on the suction side of a specially prepared compressor blade. The usage of these inserts is also required for sensor calibration. The calibration procedure is to be conducted in a flat plate test section with a fully turbulent two-dimensional boundary layer. The delta probe is flush-mounted into the flat plate surface next to a high sensitive wall shear stress balance. The wires are operated in constant temperature mode (CTA). During calibration the delta sensor is rotated by 360 degrees in steps of five degrees. For each rotation step the anemometer signals for all three wires and the signal of the balance were measured. The CTA signals were sampled with $F_s = 8192Hz$ for a measurement period of $4s$. The signals were recorded with the multichannel data acquisition system DAP 4400a. This procedure has to be conducted for different wall shear stress values which can be adjusted by varying the free stream velocity of the flat plate. The delta sensors were calibrated for wall shear stress values up to $\tau_w = 2N/mm^2$ which corresponds to a skin friction coefficient of $c_f \approx 0.006$ for the following cascade measurements. After the measurements the CTA values were temperature-compensated according to [10]. Afterwards they were plotted over the wall shear stress magnitude τ_w and the flow angle δ as shown in Fig. 1. The surface is calculated by fitting the measurements to the relation

$$E^2 = A + B\tau_w^n$$

according to the formulation published by [11]. The measurement uncertainty for the wall shear stress vector is 5% in a two-dimensional steady state flow field. During the cascade experiments the bridge voltage for all delta probes were recorded with the same sampling frequency and measurement time used during calibration. After applying the same temperature compensation as for the calibration, a look up in the corresponding calibration surface has to be done for each surface hot wire signal. These results in three different curves showing all possible combinations of wall shear stress magnitude and direction as displayed in Fig. 2. Due to the asymmetry of the cavities the three curves intersect in one single point, because all three hot wires of the delta probe are linked to the same wall shear stress vector during the measurement. In the example presented in Fig. 2 the three curves intersect at an flow angle of $\delta = 96.1°$ and a wall shear stress magnitude of $\tau_w = 1.9\,N/m^2$.

To explore the full potential of the delta probes, they have been used for wall shear stress measurements conducted at the low-speed compressor cascade test section at the department for aeronautics and astronautics at the Technische Universität Berlin. Figure 3 shows a sketch of the cascade test section. The test section is attached to the nozzle of an open wind tunnel. The discharge pressure at the outlet is matched to the ambient pressure of the laboratory. To achieve pitchwise periodic flow conditions the cascade consists of seven blades with additional tailboards at top and bottom. Boundary layer suction was applied upstream of these tailboards. The static pressure distribution at the inlet is observed with 13 pressure taps placed in each cascade sidewall. The inflow velocity profile can be controlled adjusting the volume flow rate of the boundary layer suction and the position of the tailboards. The approaching sidewall boundary layer is laminar with a displacement thickness of $\delta_1 = 4.2mm$. All measurements were conducted on the center blade of the cascade at a constant inflow velocity of $u_1 = 24.2 m/s$. This corresponds to a blade chord Reynolds number of $Re = 600,000$ and a Mach number of $Ma = 0.07$. An inflow angle variation in the range of $\beta_1 = 55^\circ - 60^\circ$ is feasible by rotating the disc the cascade is mounted to. The blade design conditions are $Re = 600,000$ and $\beta_1 = 60^\circ$. Changing the inflow angle requires an adaption of the bottom and top wall at the test section inlet as well. Figure 4 shows a sketch of the used profile geometry with the corresponding parameters summarized in Table 1. The profile geometry was especially designed for this cascade test section. The design goal for the profiles was a highly loaded blade profile with a flow turning as high as possible considering a representative pressure distribution. The c_p distribution was scaled from high subsonic flow conditions to incompressible flow conditions. This results in a flow turning of $\Delta\beta_1 = 60^\circ$. For investigations of secondary flow structure and separation phenomena a blade aspect ratio of $AR = 0.8$ was chosen for the blades. The large-scale blades allow for a simple and dense equipment of the blades with sensors to get a detailed view of the occurring flow phenomena. In addition, active flow control experiments were conducted on the cascade test section to reduce the strong secondary flow structures on the blades [12, 13]. To integrate the actuation systems a sufficient blade high is needed. However, the investigations presented here are focused on the application of the newly developed delta probes and were all carried out without the application of flow control.

For the wall shear stress measurements a special measurement blade was designed which can be equipped with 56 delta sensor inserts on the blade suction side as shown in Fig. 5. The inserts have been positioned according to preceding oil flow visualization results and the blade curvature. To avoid tripping of the laminar boundary layer in the leading edge area due to surface faceting, all delta sensors were placed in the fully turbulent flow downstream of the laminar separation bubble. The delta sensor inserts were mounted between $x/L = 23\%$ and $x/L = 70\%$ blade chord along the blade‘s midspan and in the region with strong secondary flow structures. The preceding visualization results reveal a fully separated flow downstream of $x/L = 70\%$, therefore no sensors have been placed in the trailing edge region. In the laminar flow region only standard single surface hot wires were used because of the high surface curvature in this region. They have been placed along blade midspan, because of the two dimensional flow topology in this part of the blade. The surface hot wires are mounted to a flexible printed circuit board (PCB) which was carefully integrated into the blade surface to avoid boundary layer tripping.

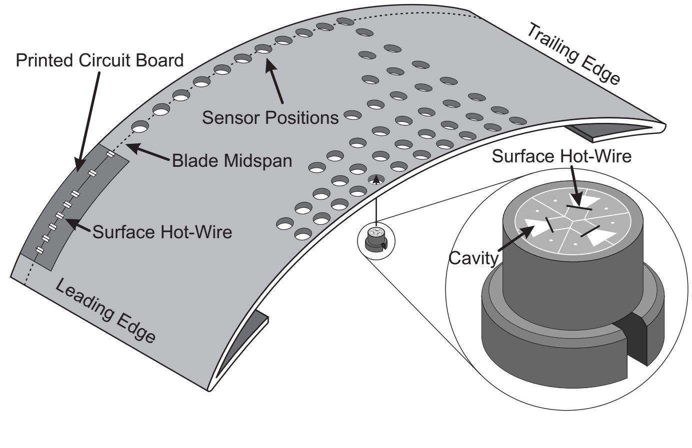

FIGURE 5: BLADE EQUIPMENT

Parameter	Value
chord length	$L = 375mm$
blade pitch	$t = 150mm$
blade height	$h = 300mm$
inflow angle	$\beta_1 = 55^\circ - 60^\circ$
flow turning	$\Delta\beta = 60^\circ$
stagger angle	$\gamma = 20^\circ$
Mach number	0.07
Reynolds number	600000
inlet turbulence	$Tu = 1.5\%$

TABLE 1: BLADE GEOMETRY DATA

Numerical Simulation

The commercial flow solver CFX [14] was used to solve the steady RANS equations. To account for the transition process on the blade surface the Gamma Theta transition model developed by Menter and Langtry [15] was employed in conjunction with the Menter SST turbulence model [16]. The Gamma Theta model is a state-of-the-art transition model in commercial CFD codes which works only in combination with the SST turbulence model. The SST turbulence model is a modified version of the BSL model [16], adding a cross-diffusion term to the specific turbulent kinetic energy in the $k-\omega$ formulation to reduce the influence of the free-stream value of ω on the results. The transition and turbulence models require a grid with more than ten grid points inside the boundary layer and a maximum wall distance of $y^+ = 2$ for the first grid cell to carefully resolve the near wall flow behavior. A plot of the numerical grid is shown in Fig. 6. The grid consists of approximately 1.65 million cells and the calculations reveal a maximum value of $y^+ = 0.7$ for the dimen-

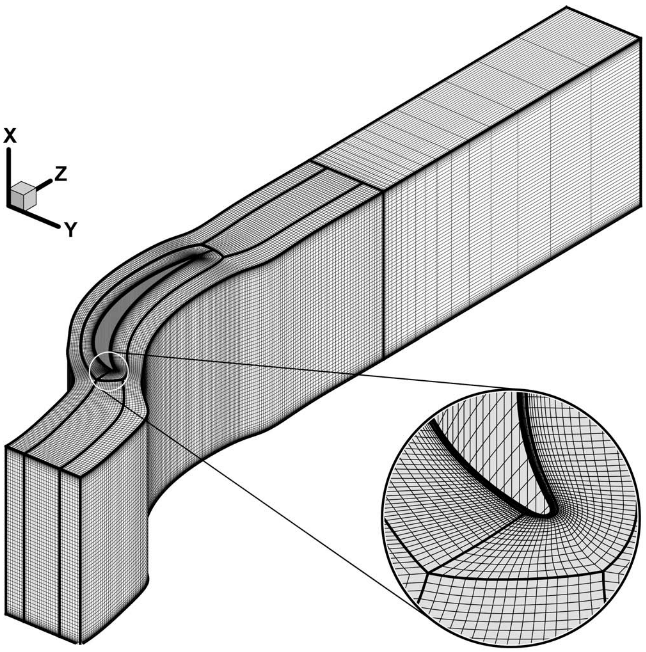

FIGURE 6: COMPUTATIONAL MESH

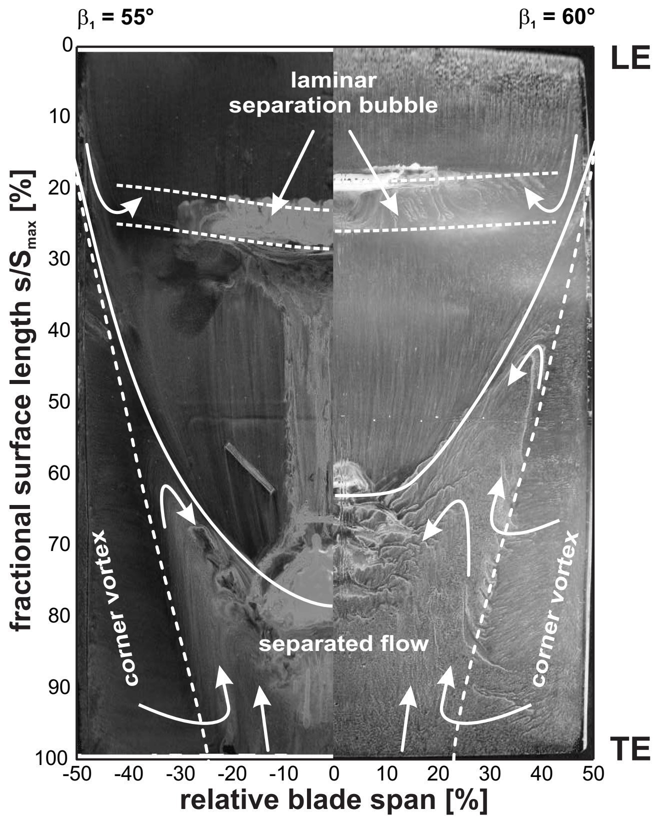

FIGURE 7: OIL FLOW VISUALIZATION

sionless wall distance. Beside the y^+ criteria also the number of grid points inside the boundary layer was controlled at selected points in the laminar and turbulent boundary layer to account for the requirements of the models used.
The boundary conditions for the simulation have been chosen according to the flow conditions in the experiments. A total pressure profile was measured at the cascade's inlet and afterwards set to the inlet plane of the numerical simulation to account for the secondary flow structures that develop in the cascade passages. Beside the total pressure profile, the total temperature and the inflow angle have been set at the inlet plain of the computational domain according to the experimental flow conditions. Only the turbulence intensity was increased for the numerical simulations to a value of $Tu = 3\%$ to resolve the turbulent reattachment sufficiently. In the simulations the average static pressure at the outlet was adapted to match the inflow Reynolds Number of the experiment.

RESULTS

Oil Flow Visualization

To position the delta sensors correctly, preliminary oil flow visualization experiments were conducted for the cascade sidewall and the blade surface. The visualization experiments were carried out on a clean blade before designing the blades for the wall shear stress measurements. Two results for the blade suction side are shown in Fig. 7. Due to the midspan symmetry of the flow field the results are plotted for a half blade span only. Figure 7 shows the result for an inflow angle of $\beta_1 = 55°$ on the left side and for $\beta_1 = 60°$ on the right side respectively. The main flow direction is from top to bottom. In the leading edge (LE) area a laminar flow region can be observed for both inflow angles. Regardless of the inflow angle, transition occurs over a laminar separation bubble as can be clearly seen by the dye accumulation between $s/S_{max} = 20\% - 30\%$. For the reduced inflow angle of $\beta_1 = 55°$ the separation bubble shifts further downstream and the streamwise length of the bubble shortens. The strong three-dimensional character of the flow in the rear blade part causes a variation of the spanwise position of the separation bubble, especially for the reduced inflow angle. Together with the laminar separation bubble the corner vortices between the blade suction side and the endwalls begin to develop. The emergence of the corner vortices causes a more and more three-dimensional evolution of the flow field after turbulent reattachment of the flow. The area of attached flow decreases in axial direction towards the trailing edge (TE). For $\beta_1 = 60°$ the flow fully separates at approximately 63% of the suction side length. Reducing the blade loading results in a downstream shift of the separation to nearly $s/S_{max} = 80\%$. The corner vortex develop-

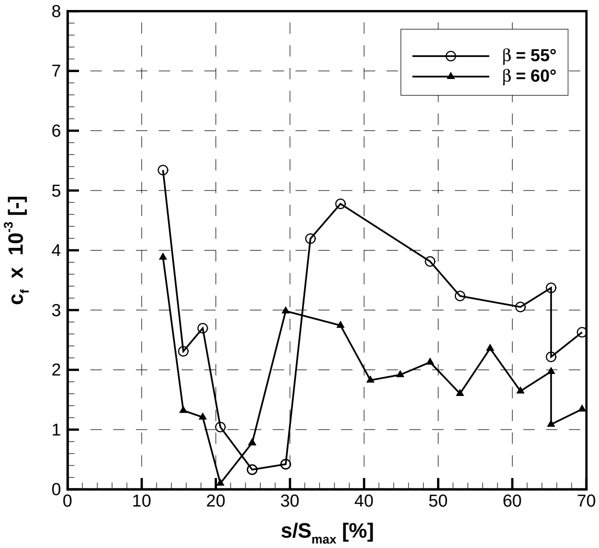

FIGURE 8: c_f DISTRIBUTION AT MIDSPAN

ment seems to be independent of the inflow angle. In both cases the corner vortices cover nearly one quarter of the blade span at the trailing edge. The delta sensor inserts were positioned between $s/S_{max} = 27\% - 70\%$ according to the oil flow visualization results and the blade curvature. A row of eleven sensors were placed at blade midspan. Due to the high blade curvature and the mainly two-dimensional flow, eight additional single surface hot wires were mounted upstream of the delta sensors as illustrated in Fig. 5. Additional 41 delta sensor were positioned in the region with a fully three-dimensional flow between the separation line and the cascade sidewall. These measurement positions were selected to prove the ability of the delta sensors to measure the flow direction and the wall shear stress magnitude in non-uniform flow fields.

Shear Stress Measurements

First the results for the midspan sensors will be discussed. After calibration, the delta sensor inserts and the single hot wires were installed on the blade‘s suction side. The first three wires of the single hot wire array, installed in the leading edge area, broke during installation. Therefore the first measurement position moves downstream to $s/S_{max} = 13\%$. The so measured non-dimensional skin friction coefficient c_f at blade midspan is shown in Fig. 8. For the calculation of the skin friction coefficient the wall shear stress τ_w is normalized with the dynamic pressure q_1 at the cascade inlet.

$$c_f = \frac{\tau_w}{q_1}$$

The results for $\beta_1 = 55°$ and $\beta_1 = 60°$ are plotted over the fractional length of the suction side s/S_{max}. The flow direction is not shown here because of the two-dimensionality of the flow at midspan. The uniform flow orientation up to the separation is shown in Fig. 7 and was also verified by the delta sensor measurements. The flow reversal below the laminar separation bubble could not be resolved, because at this blade position only single hot wires were employed. Therefore the absolute value of the wall shear stress was used to calculate the skin friction coefficient c_f. As can be expected, maximum c_f values are measured at the first sensor for both inflow angles, because of the thin boundary layer thickness despite the laminar flow that is shown by the oil flow visualization in this region. The growing boundary layer thickness results in a decreasing skin friction coefficient with increasing suction side length. During transition over the laminar separation bubble between $s/S_{max} = 20 - 30\%$ for $\beta_1 = 60°$ and $s/S_{max} = 25 - 33\%$ for $\beta_1 = 55°$ the wall shear stress magnitude reaches minimum values, characterizing separated flow. Negative c_f values caused by a backflow cannot be resolved with the single hot wires mounted in this blade region. The subsequent turbulent reattachment results in a strong shear stress increase. Further downstream the values decrease again with increasing suction side length. The fluctuations of the wall shear stress around $s/S_{max} = 60\%$, especially for $\beta_1 = 60°$, are caused by the flow separation occurring at the rear blade part. Generally higher skin friction coefficients can be observed for $\beta_1 = 55°$. Decreasing the inflow angle results in a lower blade loading and a stronger flow acceleration in the leading edge area which leads to thinner boundary layers and therefore higher wall shear stresses.

Figure 9 presents the measured c_f values and flow directions for the delta sensors located in the corner vortex region. The left side shows the results for $\beta_1 = 55°$ and the right for $\beta_1 = 60°$ respectively. The flow direction is from top to bottom. The results are plotted over the fractional suction side length and the normalized blade span whereas $\pm 50\%$ is the position of the cascade side walls. In addition to the contour plot and the arrows, the topology lines extracted from the oil flow visualization results were added to Fig. 9. High skin friction coefficients are denoted in darker colors, whereas small values are shown in lighter colors respectively. For the design case of $\beta_1 = 60°$ mainly small c_f values can be observed except close to the sidewall. This indicates that the flow is separated over a large portion of the observed flow region. This observation can be confirmed by the oil flow visualization. In addition to the magnitude, the measured wall shear stress directions are depicted with arrows. There is a segmentation in three groups of arrows. The first includes the arrows in the corner vortex region between the sidewall and the dashed corner vortex line, marked with (I). The second group (II) is located between the dashed line of the corner vortex and the solid line which marks the turbulent flow separation. The last group of arrows includes the sensors within the attached flow on the

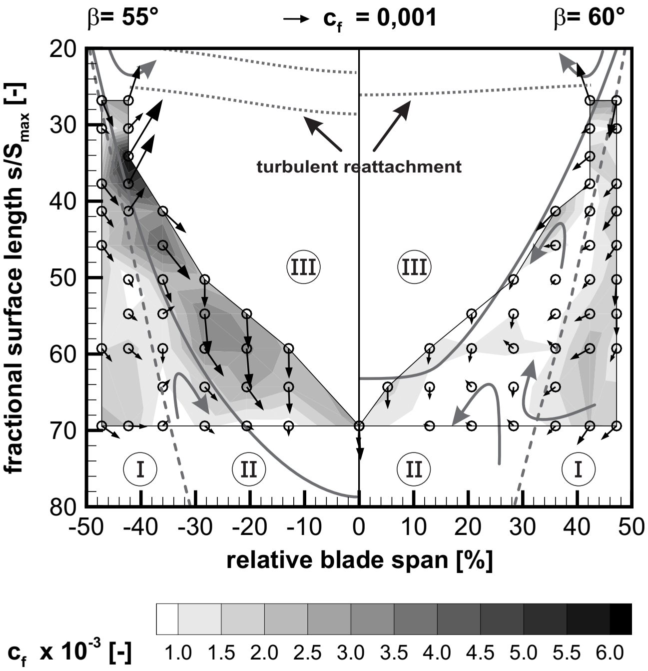

FIGURE 9: c_f DISTRIBUTION AND FLOW DIRECTION ON THE BLADE SUCTION SIDE

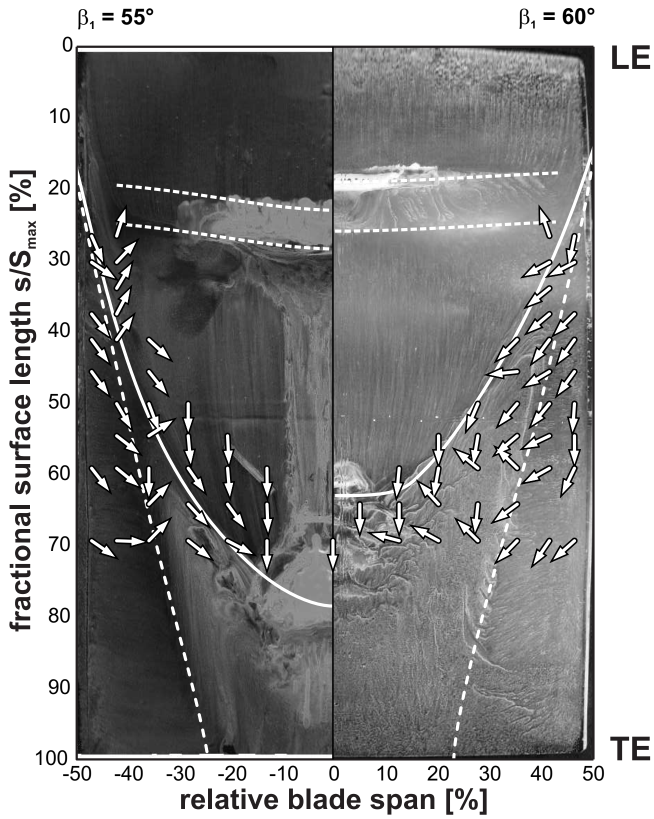

FIGURE 10: MEASURED FLOW DIRECTION AND OIL FLOW VISUALIZATION

blade suction side (III). In the corner vortex region (I) most of the arrows show a flow direction directed away from the sidewall which can be expected for the corner vortices, because of the known direction of rotation for these vortices. For the second group (II) within the flow separation no distinct flow direction can be observed due to the non-uniform flow structures in this region. This means for the delta sensors that the three single hot wires are no longer linked to the same wall shear stress vector. Slightly different wall shear stress magnitudes and directions between the individual wires result in poor correlations and a strong increase of the measurement error. This is caused by the large diameter of the delta sensors compared to the flow structures in this region. Therefore no exact conclusions can be made for the wall shear stress direction in separated flows [1]. For an exact determination of the wall shear stress vector uniform flow conditions are needed at the measurement location. However, this limitation can be overcome by further reducing the sensor by means of MEMS technology demonstrated, for example, in [17]. Nevertheless the presented results show the ability of the newly designed delta sensors to measure the wall shear stress magnitude and direction in complex flows. In the last region it can be seen that most arrows point to the trailing edge. The flow is attached and mainly two.dimensional; except for the arrow close to the laminar separation bubble which is oriented in the opposite direction. At this position there is a close interaction between the laminar separation bubble and the developing corner vortex. A comparison of the measured wall shear stress direction with the results of the oil flow visualization shows good agreement (Fig. 10). The results for the reduced inflow angle confirm these findings. Decreasing the blade loading causes a reduction of the separated flow area. Section (II) in Fig. 9 is significantly smaller. By contrast, section (III) has extended towards the trailing edge. Significantly higher c_f can be observed in this region compared to section (II). The flow is mainly oriented to the trailing edge except for the area close to the separation line, where the wall shear stress direction is parallel to the separation line. As already described for $\beta_1 = 60°$, the two top arrows that are closest to the separation bubble are reversed due to interaction of the separation bubble with the corner vortices. Downstream of these two measurement positions the maximum wall shear stress values can be observed in conjunction with two arrows pointing towards the leading edge. Analyzing the RMS values presented in Fig. 11 reveals maximum values for this sensor positions as well. This indicates strong flow fluctuations which makes an exact determination of the flow direction difficult like in the region of separated flow. Nevertheless, in the area of the corner vor-

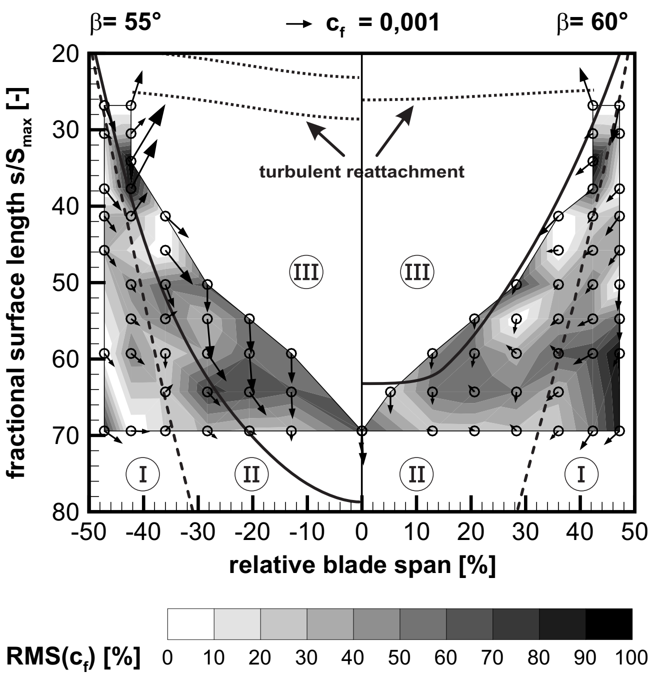

FIGURE 11: $RMS(c_f)$ DISTRIBUTION AND FLOW DORECTION ON THE BLADE SUCTION SIDE

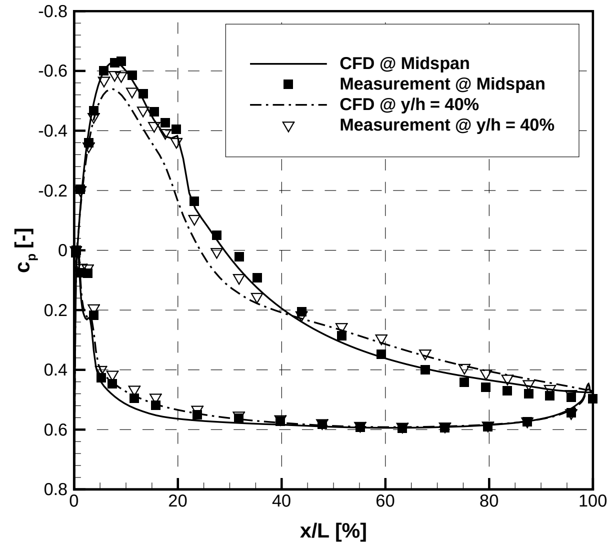

FIGURE 12: COMPARISON OF THE c_p DISTRIBUTION FOR $\beta_1 = 60°$

tex (I) increased c_f values (Fig. 9) can be observed compared to section(II) together with a uniform flow direction tilted away from the sidewall as already observed for $\beta_1 = 60°$. The good agreement between the delta sensor results and the oil flow visualization can be confirmed for $\beta_1 = 55°$ as well (Fig. 10).

Numerical Simulation

In addition to the measurements numerical simulations with the commercial flow solver CFX were performed for the compressor cascade. For the simulations the inflow angle was set to $\beta_1 = 60°$ and the outlet pressure was varied to match the chord Reynolds number of the experimental investigations. Beside the presented data, detailed pressure measurements for the hole blade surface were conducted in earlier investigations [12]. Therefore a detailed database is available for comparison with the numerical results. First a comparison of the normalized pressure distribution c_p is undertaken to prove the general quality of the numerical simulations. c_p is calculated by normalizing the local pressure difference with the dynamic pressure at the cascade inlet.

$$c_p = \frac{p - p_1}{p_t - p_1}$$

Where p_1 stands for the static pressure at the inlet and p_t for the total pressure respectively. Figure 12 shows the c_p distribution for midspan and for a relative blade height of $y/h = 40\%$. The agreement of the results is rather good, especially at blade's midspan. The position of the laminar separation bubble, clearly recognizable by the pressure plateau on the blade's suction side at a $x/L = 20\%$, is fairly good predicted by the applied Gamma Theta transition model. The pressure plateau is even visible in the results of the numerical simulation. Downstream of the turbulent reattachment a faster pressure recovery can be observed for the numerical results, but the deviation from the experiment is minor. The leading edge separation bubble on the pressure side is also resolved by the numerical simulations, therefore a good match is found for the pressure side as well, whereas small differences in the c_p distribution can be detected for the suction side at a spanwise position of $y/h = 40\%$ (close to the sidewall). The suction peak is less distinct in the numerical results and a pressure plateau caused by the separation bubble is no longer present as shown by the experimental data. Nevertheless, a good agreement between the numerical and experimental results can be observed downstream of $x/L = 40\%$. A good match is also available for the pressure side results. Despite the small differences in the pressure distribution close to the sidewalls the numerical model has captured most of the spanwise flow patterns on the blade surface induced by the three-dimensionality of the flow. Therefore further comparisons can be made for the direction and the magnitude of the wall shear stress. Figure 13 shows the c_f distributions at blade midspan for an inflow angle of $\beta_1 = 60°$.

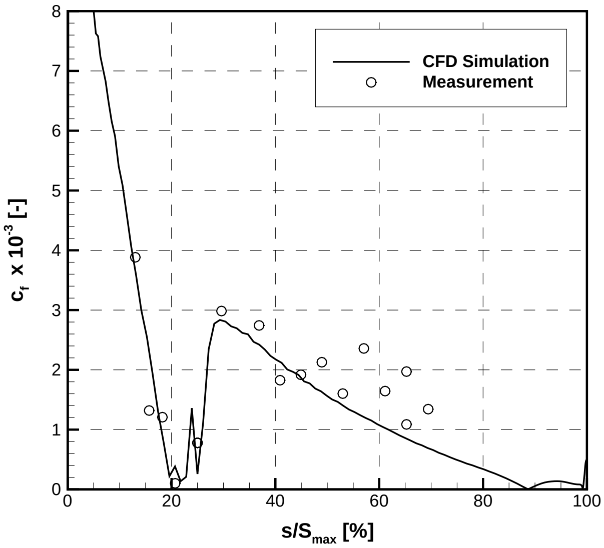

FIGURE 13: COMPARISON OF THE c_f DISTRIBUTION AT MIDSPAN FOR $\beta_1 = 60°$

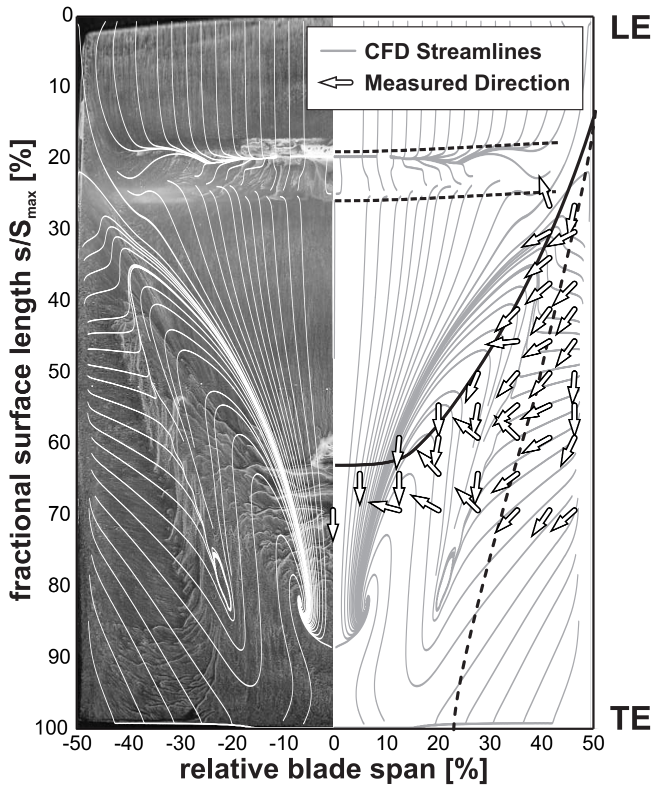

FIGURE 14: STREAMLINES AND MEASURED FLOW DIRECTION ON THE BLADE SUCTION SIDE

For reasons of comparison the absolute values of c_f were plotted for the numerical results as well. Therefore no backflow can be observed at the position of the laminar separation bubble. Again a fairly good agreement between the experimental and numerical results can be observed, especially in the leading edge part of the blade. As already seen in the pressure distribution the position of the laminar separation bubble between $s/S_{max} = 18\%$ and $s/S_{max} = 27\%$ is well predicted in the simulation. The differences in c_f are within the measurement tolerances. Larger differences are only observed downstream of $s/S_{max} = 55\%$ due to the beginning flow separation. As already noted before, an exact measurement of the wall shear stress within separated flow is rather difficult with the delta sensors.

To compare the wall shear stress direction, surface streamlines computed from the numerical results are shown in Fig. 14. The left part of Fig. 14 shows the streamlines on top of the oil flow visualization image for $\beta_1 = 60°$. Again the good prediction of the laminar separation bubble becomes clear. Downstream of the separation bubble some differences are found in the region of the corner vortex. This has already been observed in the pressure distribution. The development of the corner vortex is overpredicted by the simulation. The streamlines show corner vortices that cover approximately 35% of the relative blade height at the trailing edge. The analysis of the underlying oil flow visualization reveals only a spanwise extension of 25% (Fig. 7). This overprediction leads to an increased passage blockage in the simulation and a stronger narrowing of the attached flow in the middle of the blade. Therefore the numerical results show a turbulent flow separation line which is curved to the right instead of to the left as can be inferred from the oil flow visualization. The right half of Fig. 14 clarifies this finding. The CFD surface streamlines, colored in grey, are plotted together with the experimental results of the oil flow visualization and the delta sensor measurements. Distinct differences can be observed in the orientations of the separation lines comparing the black topology lines of the flow visualization with the numerically calculated surface streamlines. Furthermore the numerical results reveal flow separation extending further downstream at blade‘s midspan compared to the measurements. The flow remains attached until $s/S_{max} \approx 85\%$ whereas the experiments show a fully separated flow at $s/S_{max} \approx 65\%$. This explains the bigger differences in the c_f distribution for blade midspan beyond $s/S_{max} = 55\%$ in Fig. 13 as well. Nevertheless, in the region of the corner vortex the overall flow pattern is captured, even when there are some differences between the calculated flow directions and the measured flow angles, whereas large differences can be observed in the region of separated flow because of the mismatch among the separation lines and the larger measurement error of the delta sensors in separated flows.

CONCLUSION

A newly designed wall shear stress sensor based on the thermoelectrical principle is presented and validated for turbomachine measurements. A layout of three single hot wires mounted above a small asymmetric cavity allows for the measurement of magnitude and direction of the shear stress distribution. The so-called delta probes were tested in a strongly three-dimensional compressor cascade flow field to prove their ability to measure all three components of the wall shear stress vector. For these measurements the probes were mounted on a blade‘s suction side of a highly loaded large scale compressor cascade. Visualization results obtained in preceding measurements reveal a strong three-dimensional flow topology on the blade‘s suction sides and were employed to position the delta sensors on the blade surface. Furthermore, numerical flow simulations were carried out for the observed flow case with the commercial flow solver CFX. The comparison of the oil flow visualization results with the measured wall shear stress directions of the delta sensor shows a high degree of agreement in the regions of attached flow. Only in separated flows an exact measurement of flow direction and wall shear stress magnitude is difficult. The numerical results confirm the suitability of the delta sensors to measure the wall shear stress direction and magnitude in complex flow fields.

ACKNOWLEDGMENT

The delta sensors were developed within the framework of the priority programme 1147, *Imaging Measurements Methods for Flow Analysis*, funded by the German Research Foundation (DFG). The authors would like to thank for the support of the work and the funding.

REFERENCES

[1] Dobriloff, C., and Nitsche, W., 2008. “Delta surface hot-wires as a means of measuring wall shear stresses at arbitrary flow directions”. In XXII ICTAM, Adelaide, Australia.

[2] Haritonidis, J., 1989. “The measurement of wall shear stress”. *Advances in fluid mechanics measurements*, pp. 229–261.

[3] Winter, K., 1977. “An outline of the techniques available for the measurement of skin friction in turbulent boundary layers”. *Progress in Aerospace Sciences,* ***18***, pp. 1–57.

[4] Sieverding, C. H., Arts, T., Dénos, R., and Brouckaert, J.-F., 2000. “Measurement techniques for unsteady flows in turbomachines”. *Experiments in Fluids,* ***28***, pp. 285–321.

[5] Hodson, H. P., Huntsman, I., and Steele, A. B., 1994. “An investigation of boundary layer development in a multistage lp turbine”. *ASME Journal of Turbomachinery,* ***116***, pp. 375–383.

[6] McCroskey, W., and Durbin, E., 1972. “Flow angle and shear stress measurements using heated films and wires”. *Journal of Basic Engineering*, pp. 46–52.

[7] Sumer, B., Arnskov, M., Christiansen, N., and Jorgensen, F., 1993. “Two-component hot-film probe for measurements of wall shear stress”. *Experiments in Fluids,* ***15***, pp. 380–384.

[8] Dobriloff, C., and Nitsche, W., 2009. “Surface pressure and wall shear stress measurements on a wall mounted cylinder”. *Notes an Numerical Fluid Mechanics and Multidisciplinary Design,* ***106***, pp. 197–206.

[9] Sturzebecher, D., Anders, S., and Nitsche, W., 2001. “The surface hot wire as a means of measuring mean and fluctuating wall shear stress”. *Experiments in Fluids,* ***31***(3), Sept., pp. 294–301.

[10] Bruun, H., 1995. *Hot-Wire Anemometry - Principles and Signal Analysis*. Oxford Science Publications.

[11] Hanratty, T., and Campbell, J., 1983. *Fluid Mechanics Measurements*. Hemisphere, ch. Measurements of wall shear stress, pp. 559–615.

[12] Zander, V., Hecklau, M., Nitsche, W., Huppertz, A., and Swoboda, M., 2009. “Active control of corner vortices on a highly loaded compressor cascade”. In 8th European Turbomachinery Conference, Graz.

[13] Hecklau, M., Zander, V., Nitsche, W., Huppertz, A., and Swoboda, M., 2010. “Active secondary flow control on a highly loaded compressor cascade by periodically pulsating jets”. In New Results in Numerical and Experimental Fluid Mechanics VII - NNFM, Vol. 112, Springer, pp. 199–207.

[14] ANSYS EUROPE LTD., 2005. *ANSYS CFX-Solver, Release 10.0: Theory*.

[15] Menter, F., Langtry, R., Likki, S. R., Suzen, Y., Huang, P., and Völker, S., 2006. “A correlation-based transition model using local variables - part i: Model formulation”. *ASME Journal of Turbomachinery,* ***128***, pp. 413–422.

[16] Menter, F., 1994. “Two-equation eddy-viscosity turbulence models for engineering applications”. *AIAA JOURNAL,* ***32***(8), pp. 1598–1605.

[17] Burkhardt, O., Dinata, U., Warsop, C., and Nitsche, W., 2000. “New developments in surface flow sensor technology within the framework of aeromems”. In Proceeding of the European Conference Potsdam 2000 by CEAS/DragNet, Notes on Numerical Fluid Mechanics.